Electronic Supplementary Information (ESI)

Strong *in vitro* anticancer activity of copper(II) and zinc(II) complexes containing naturally occurring Lapachol: Cellular effects in ovarian A2780 cells

Sara Stocchetti,[a,b] Ján Vančo,[a], Jan Belza,[a] Zdeněk Dvořák,[c] Zdeněk Trávníček [a,*]

[a] Czech Advanced Technology and Research Institute, Regional Centre of Advanced Technologies and Materials, Palacký University, Šlechtitelů 27, CZ-779 00 Olomouc, Czech Republic.

[b] University of Pisa, Dipartimento di Chimica e Chimica Industriale, Via G. Moruzzi 13, I-56124 Pisa, Italy.

[c] Department of Cell Biology and Genetics, Faculty of Science, Palacký University, Šlechtitelů 27, CZ-779 00 Olomouc, Czech Republic.

The authors would like to dedicate this work to Jan Belza, our beloved colleague and friend, who passed away unexpectedly on February 15, 2024, at the age of 31 years.

* Correspondence: zdenek.travnicek@upol.cz ; Tel.: +420 585 634 545.

Table of Contents	Page
Fig. S1 ESI-MS spectrum of complex **1** measured in MeOH using the positive ionisation mode immediately after the sample dissolution.	S4
Fig. S1a The isotopic resolved part of the ESI/MS spectra of complex **1** measured in MeOH in the region involving the peak at 636.33 *m/z*, corresponding to $[Cu(Lap)(bphen)]^+$ (the red bordered inset represents the theoretical isotopic distribution pattern for this species).	S4
Fig. S1b The isotopic resolved part of the ESI/MS spectra of complex **1** measured in MeOH in the region involving the peak at 727.41 *m/z*, corresponding to $[Cu(bphen)_2]^+$ (the red bordered inset represents the theoretical isotopic distribution pattern for this species).	S5
Fig. S2 ESI-MS spectrum of complex **2** measured in MeOH using the positive ionisation mode immediately after the sample dissolution.	S5
Fig. S2a The isotopic resolved part of the ESI/MS spectra of complex **2** measured in MeOH in the region involving the peak at 498.25 *m/z*, corresponding to $[Cu(Lap)(mphen)]^+$ (the red bordered inset represents the theoretical isotopic distribution pattern for this species).	S6
Fig. S3 ESI-MS spectrum of complex **3** measured in MeOH using the positive ionisation mode immediately after the sample dissolution.	S6
Fig. S3a The isotopic resolved part of the ESI/MS spectra of complex **3** measured in MeOH in the region involving the peak at 460.24 *m/z*, corresponding to $[Cu(Lap)(bpy)]^+$ (the red bordered inset represents the theoretical isotopic distribution pattern for this species).	S7
Fig. S4 ESI-MS spectrum of complex **4** measured in MeOH using the positive ionisation mode immediately after the sample dissolution.	S7
Fig. S4a The isotopic resolved part of the ESI/MS spectra of complex **4** measured in MeOH in the region involving the peak at 537.35 *m/z*, corresponding to $[Cu(Lap)(terpy)]^+$ (the red bordered inset represents the theoretical isotopic distribution pattern for this species).	S8
Fig. S5 ESI-MS spectrum of complex **5** measured in MeOH using the positive ionisation mode immediately after the sample dissolution.	S8
Fig. S5a The isotopic resolved part of the ESI/MS spectra of complex **5** measured in MeOH in the region involving the peak at 637.37 *m/z*, corresponding to $[Zn(Lap)(bphen)]^+$ (the red bordered inset represents the theoretical isotopic distribution pattern for this species).	S9
Fig. S5b The isotopic resolved part of the ESI/MS spectra of complex **5** measured in MeOH in the region involving the peak at 969.59 *m/z*, corresponding to $[Zn(Lap)(bphen)_2]^+$ (the red bordered inset represents the theoretical isotopic distribution pattern for this species).	S9
Fig. S6 ESI-MS spectrum of complex **6** measured in MeOH using the positive ionisation mode immediately after the sample dissolution.	S10
Fig. S6a The isotopic resolved part of the ESI/MS spectra of complex **6** measured in MeOH in the region involving the peak at 499.29 *m/z*, corresponding to $[Zn(Lap)(mphen)]^+$ (the red bordered inset represents the theoretical isotopic distribution pattern for this species).	S10
Fig. S6b The isotopic resolved part of the ESI/MS spectra of complex **6** measured in MeOH in the region involving the peak at 693.39 *m/z*, corresponding to $[Zn(Lap)(mphen)_2]^+$ (the red bordered inset represents the theoretical isotopic distribution pattern for this species).	S11
Fig. S7 ESI-MS spectrum of complex **7** measured in MeOH using the positive ionisation mode immediately after the sample dissolution.	S11
Fig. S7a The isotopic resolved part of the ESI/MS spectra of complex **7** measured in MeOH in the region involving the peak at 485.27 *m/z*, corresponding to $[Zn(Lap)(phen)]^+$ (the red bordered inset	S12

represents the theoretical isotopic distribution pattern for this species).	
Fig. S7b The isotopic resolved part of the ESI/MS spectra of complex **7** measured in MeOH in the region involving the peak at 665.35 *m/z*, corresponding to $[Zn(Lap)(phen)_2]^+$ (the red bordered inset represents the theoretical isotopic distribution pattern for this species).	S12
Fig. S8 IR spectrum of free Lapachol (HLap).	S13
Fig. S9 IR spectrum of complex **1**.	S13
Fig. S10 IR spectrum of complex **2**.	S14
Fig. S11 IR spectrum of complex **3**.	S14
Fig. S12 IR spectrum of complex **4**.	S15
Fig. S13 IR spectrum of complex **5**.	S15
Fig. S14 IR spectrum of complex **6**.	S16
Fig. S15 IR spectrum of complex **7**.	S16
Fig. S16 Electronic spectra of complex **1** measured in the solid state (red solid line) and MeOH (red dashed line).	S17
Fig. S17 ESI-MS spectrum of complex 1 measured in MeOH:H_2O (1:1) using the positive ionisation mode immediately after the sample preparation.	S17
Fig. S18 ESI-MS spectrum of complex 1 measured in MeOH:H_2O (1:1) using the positive ionisation mode 24 h after the sample preparation.	S18
Fig. S19 ESI-MS spectrum of complex 5 measured in MeOH:H_2O (1:1) using the positive ionisation mode immediately after the sample preparation.	S18
Fig. S20 ESI-MS spectrum of complex 5 measured in MeOH:H_2O (1:1) using the positive ionisation mode 24 h after the sample preparation.	S19
Table S1 Crystal data and structure refinements for **4**, **5,** and **6**	S20
Fig. S21 The O–H···O hydrogen bonds (cyan dashed lines) connect centrosymmetrically two individual molecules of **4** through the nitrate anions.	S21
Table S2 Parameters of selected hydrogen bonds [Å and °] in complex **4**.	S21
Fig. S22 Part of the crystal structure of **5**, showing the C–H···C and C–H···O non-covalent contacts (red dotted lines) connecting individual molecules of **5** into a 3D structure.	S22
Table S3 Parameters of selected hydrogen bonds [Å and °] in complex **5**.	S22
Fig. S23 Part of the crystal structure of **6**, showing the C–H···C, C–H···O (red dotted lines) and C···O (cyan dotted lines) non-covalent contacts, connecting individual molecules of **6** into a 3D structure.	S23
Table S4 Parameters of selected hydrogen bonds [Å and °] for complex **6**.	S23
Fig. S24 The cyclic-voltammograms of complexes **2**, **3**, **5**, and ligand lapachol measured at 0.1 mM concentration in CH_2Cl_2 containing 0.1 M Bu_4NPF_6 as a supporting electrolyte using the Gamry Series G300 potentiostat (Gamry Instruments, Warminster, PA, USA) equipped with platinum foil working and counter electrode and Ag/AgCl in saturated KOH reference electrode.	S24
Table S5 The potentials (V) of the maxima/shoulders of the anodic and cathodic waves (E_{pa} - anodic, E_{pc} - cathodic) vs. reference electrode Ag/AgCl in saturated KOH. The values were obtained by the analysis of the raw data using the Gamry Echem Analyst software (ver. 6.33).	S24

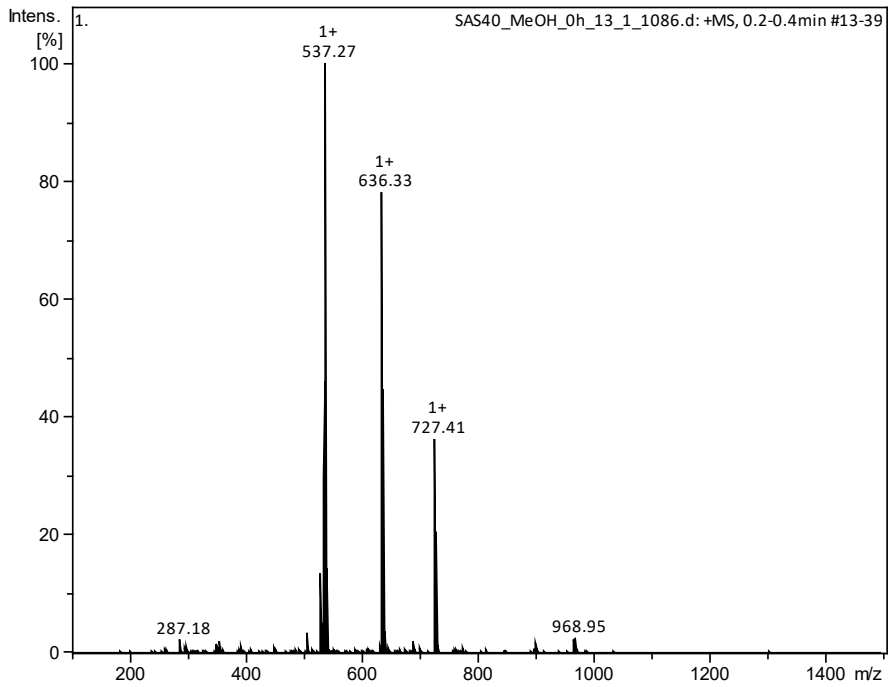

Fig. S1 ESI-MS spectrum of complex **1** measured in MeOH using the positive ionisation mode immediately after the sample dissolution. The main peaks represent the following pseudomolecular ions (theor. monoisotopic mass): 636.33 *m/z* $[Cu(Lap)(bphen)]^+$ (636.15); 727.41 *m/z* $[Cu(bphen)_2]^+$ (727.19).

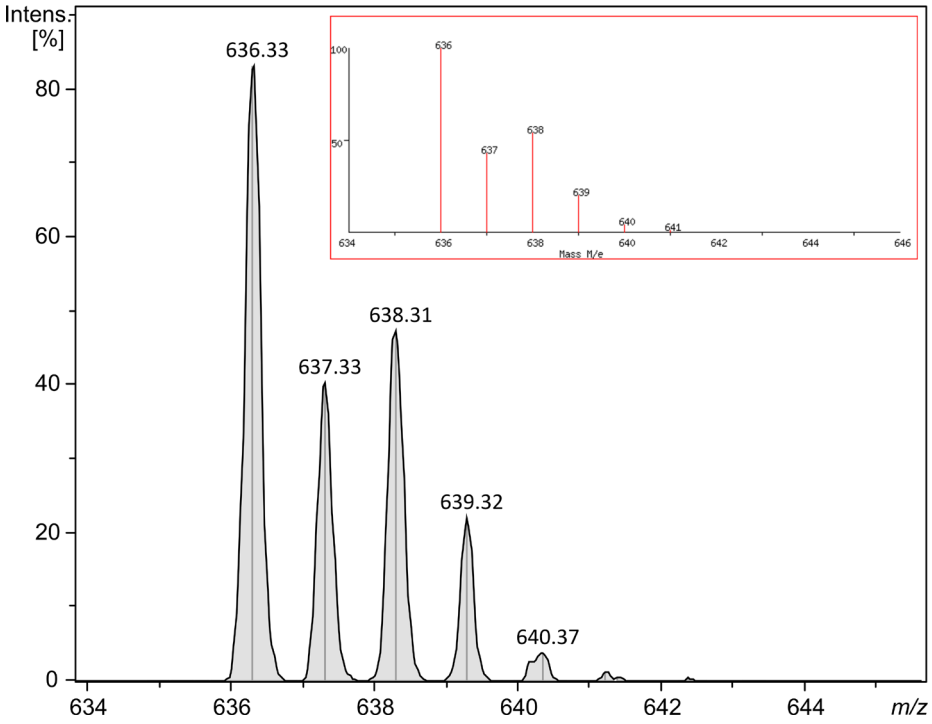

Fig. S1a The isotopic resolved part of the ESI/MS spectra of complex **1** measured in MeOH in the region involving the peak at 636.33 *m/z*, corresponding to $[Cu(Lap)(bphen)]^+$ (the red bordered inset represents the theoretical isotopic distribution pattern for this species).

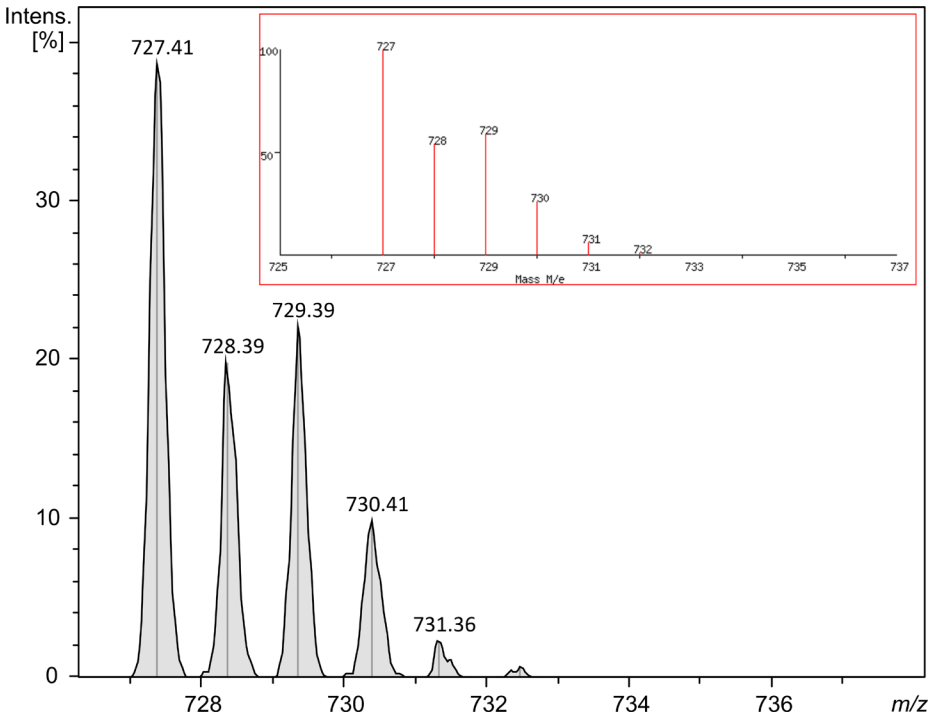

Fig. S1b The isotopic resolved part of the ESI/MS spectra of complex **1** measured in MeOH in the region involving the peak at 727.41 *m/z*, corresponding to $[Cu(bphen)_2]^+$ (the red bordered inset represents the theoretical isotopic distribution pattern for this species).

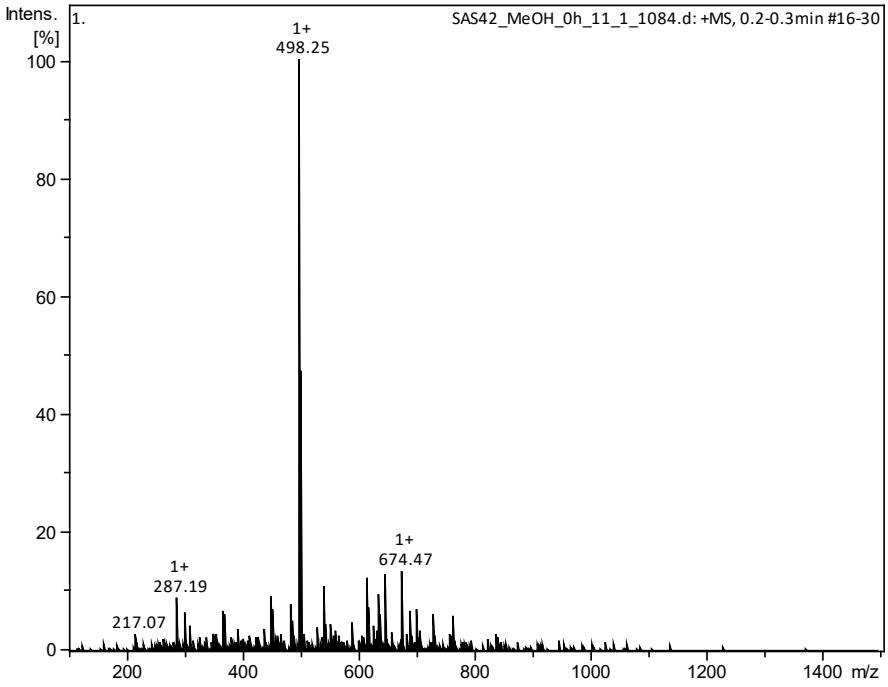

Fig. S2 ESI-MS spectrum of complex **2** measured in MeOH using the positive ionisation mode immediately after the sample dissolution. The main peak represents the following pseudomolecular ion (theor. monoisotopic mass): 498.25 *m/z* $[Cu(Lap)(mphen)]^+$ (498.10).

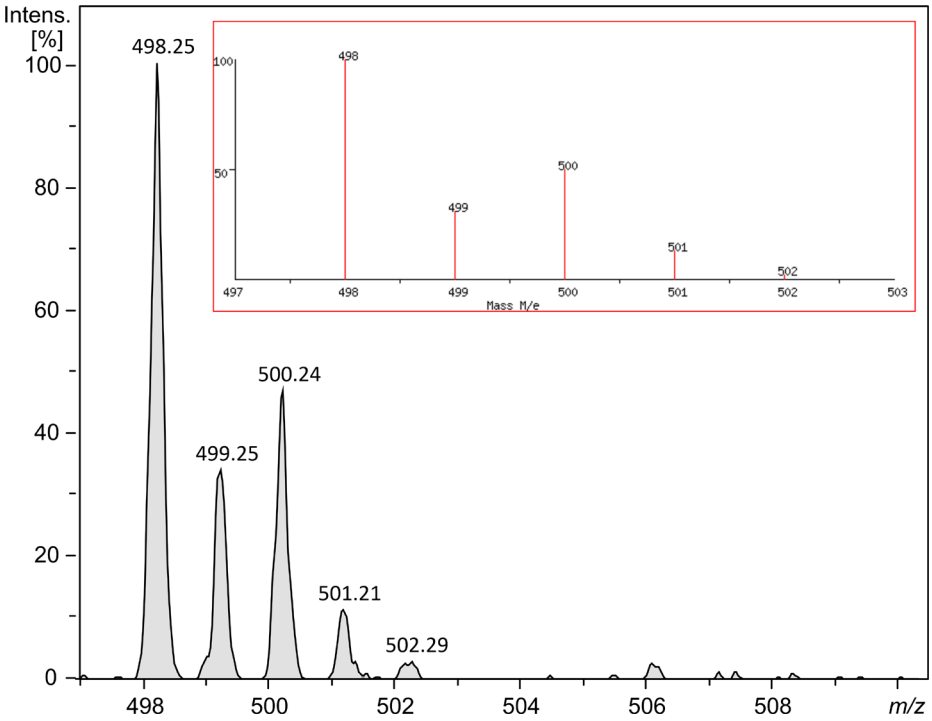

Fig. S2a The isotopic resolved part of the ESI/MS spectra of complex **2** measured in MeOH in the region involving the peak at 498.25 *m/z*, corresponding to $[Cu(Lap)(mphen)]^+$ (the red bordered inset represents the theoretical isotopic distribution pattern for this species).

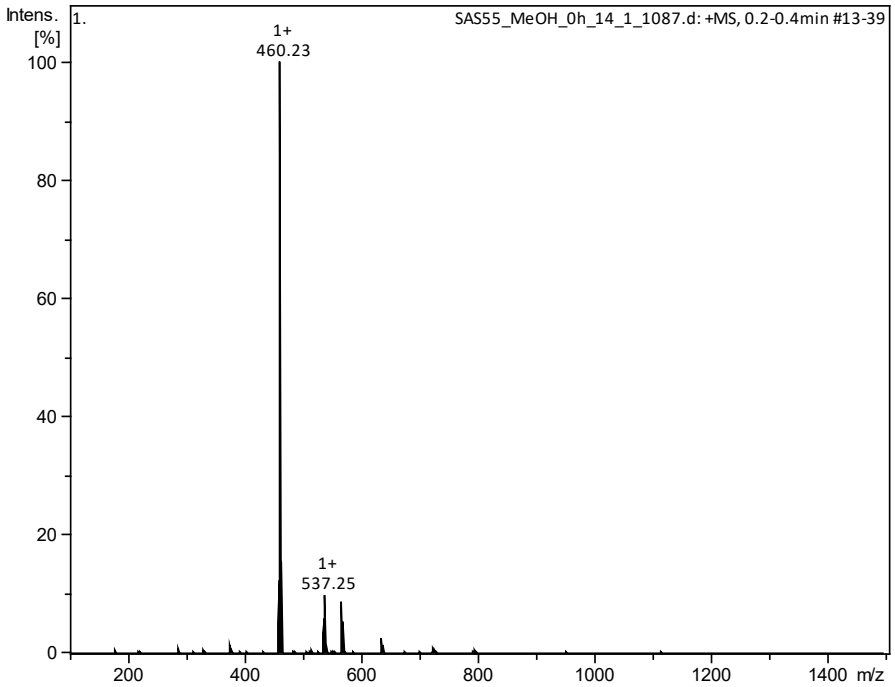

Fig. S3 ESI-MS spectrum of complex **3** measured in MeOH using the positive ionisation mode immediately after the sample dissolution. The main peak represents the following pseudomolecular ion (theor. monoisotopic mass): 460.23 *m/z* $[Cu(Lap)(bpy)]^+$ (460.08).

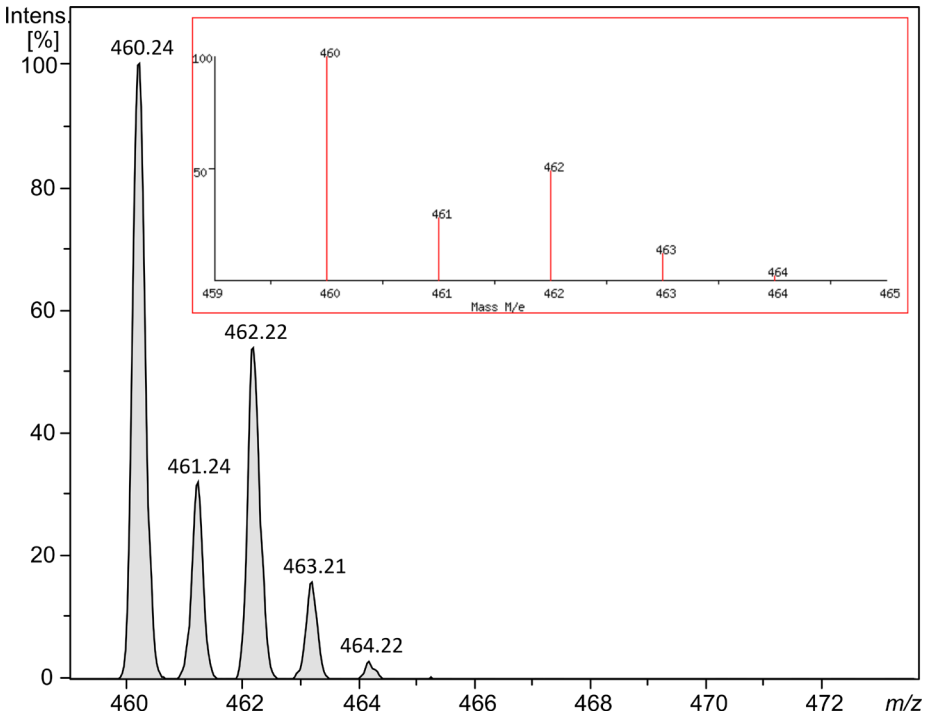

Fig. S3a The isotopic resolved part of the ESI/MS spectra of complex **3** measured in MeOH in the region involving the peak at 460.24 *m/z*, corresponding to $[Cu(Lap)(bpy)]^+$ (the red bordered inset represents the theoretical isotopic distribution pattern for this species).

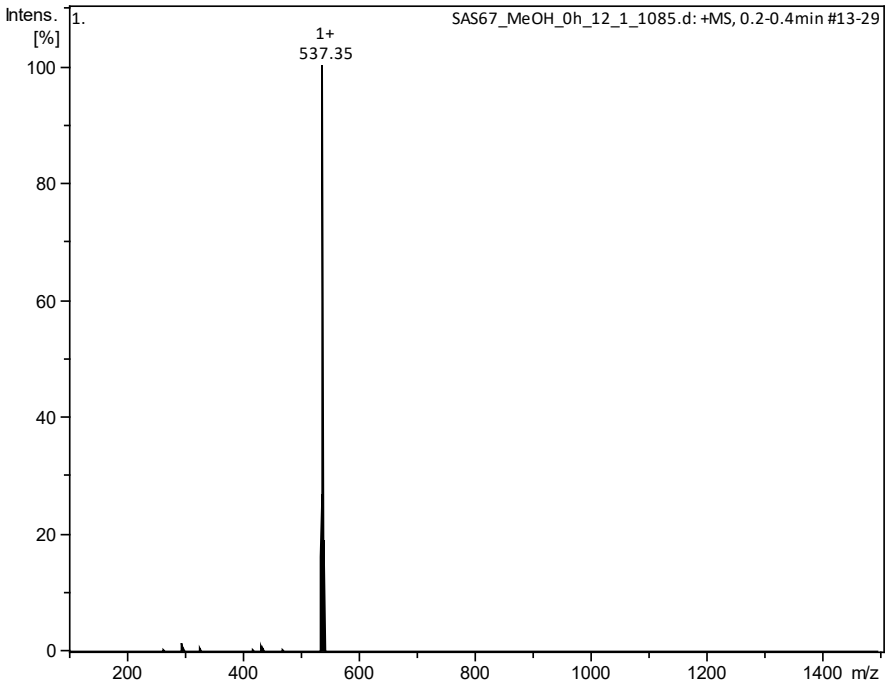

Fig. S4 ESI-MS spectrum of complex **4** measured in MeOH using the positive ionisation mode immediately after the sample dissolution. The main peak represents the following pseudomolecular ion (theor. monoisotopic mass): 537.35 *m/z* $[Cu(Lap)(terpy)]^+$ (537.11).

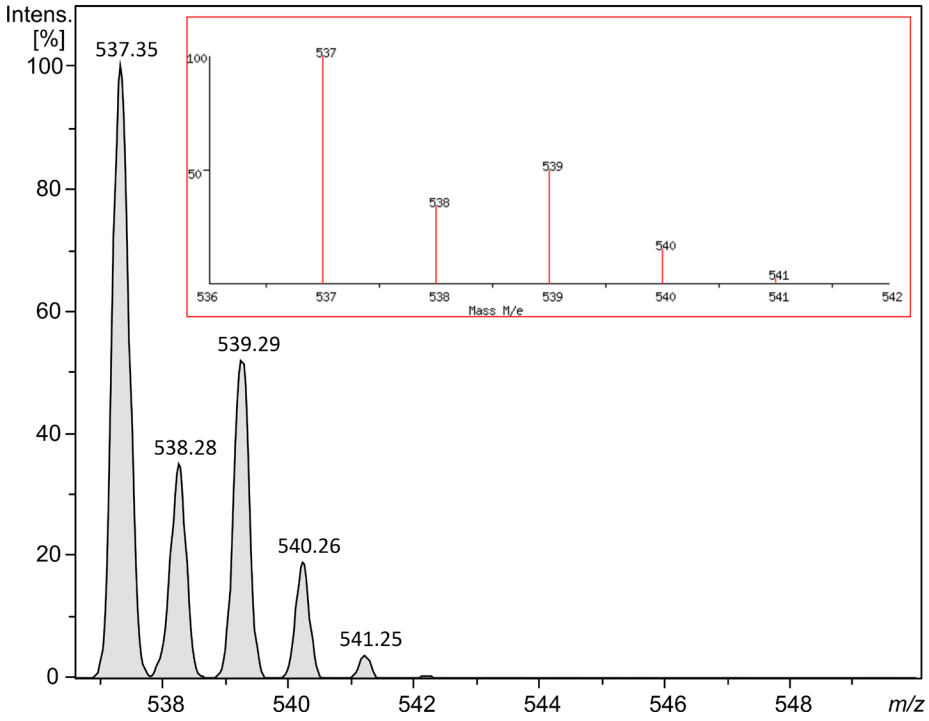

Fig. S4a The isotopic resolved part of the ESI/MS spectra of complex **4** measured in MeOH in the region involving the peak at 537.35 *m/z*, corresponding to $[Cu(Lap)(terpy)]^+$ (the red bordered inset represents the theoretical isotopic distribution pattern for this species).

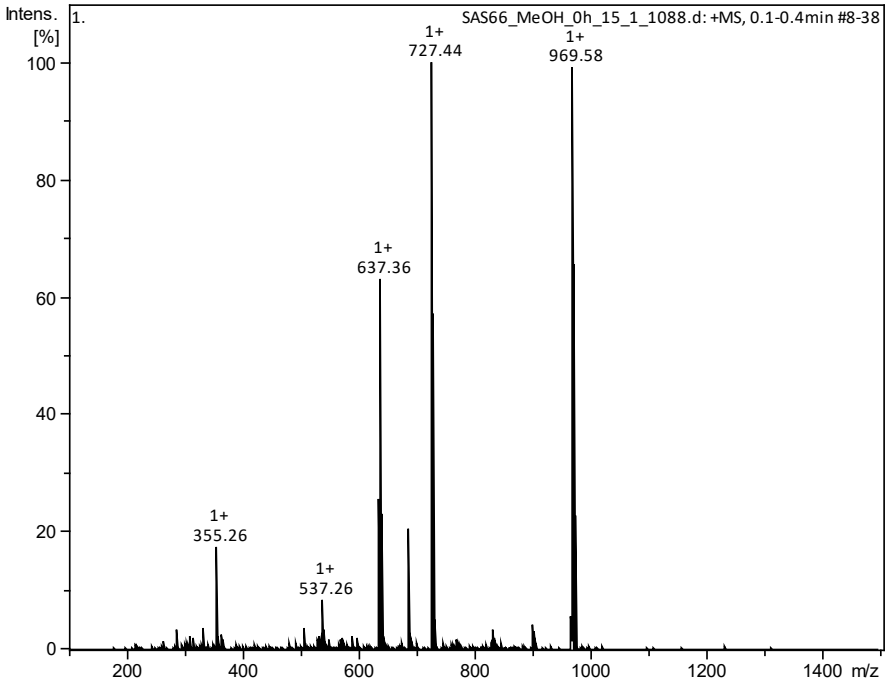

Fig. S5 ESI-MS spectrum of complex **5** measured in MeOH using the positive ionisation mode immediately after the sample dissolution. The main peaks represent the following pseudomolecular ions (theor. monoisotopic mass): 637.36 *m/z* $[Zn(Lap)(bphen)]^+$ (637.15); 969.58 *m/z* $[Zn(Lap)(bphen)_2]^+$ (969.28).

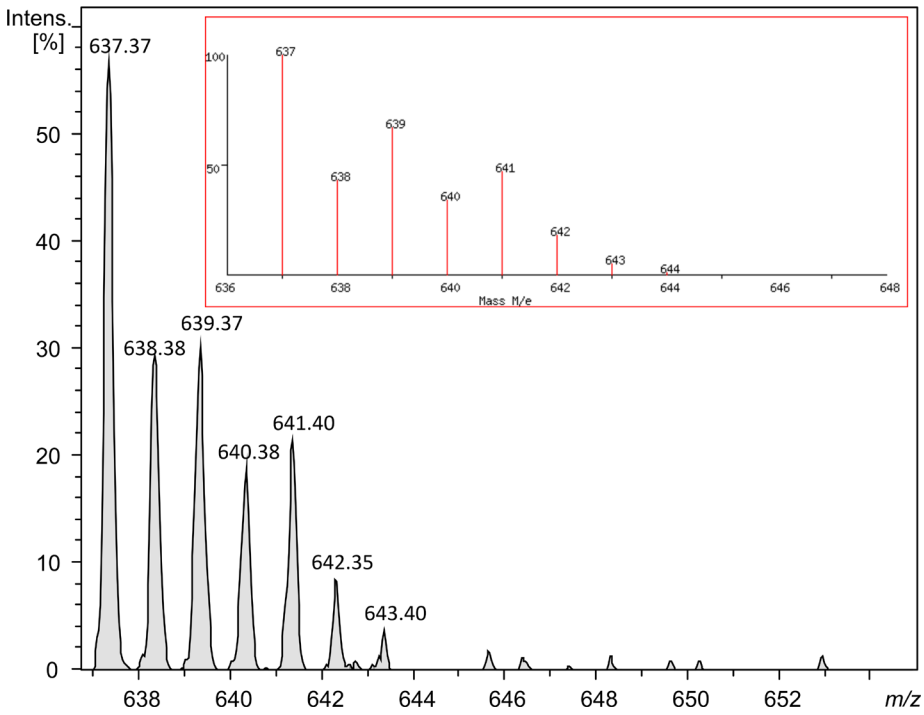

Fig. S5a The isotopic resolved part of the ESI/MS spectra of complex **5** measured in MeOH in the region involving the peak at 637.37 *m/z*, corresponding to $[Zn(Lap)(bphen)]^+$ (the red bordered inset represents the theoretical isotopic distribution pattern for this species).

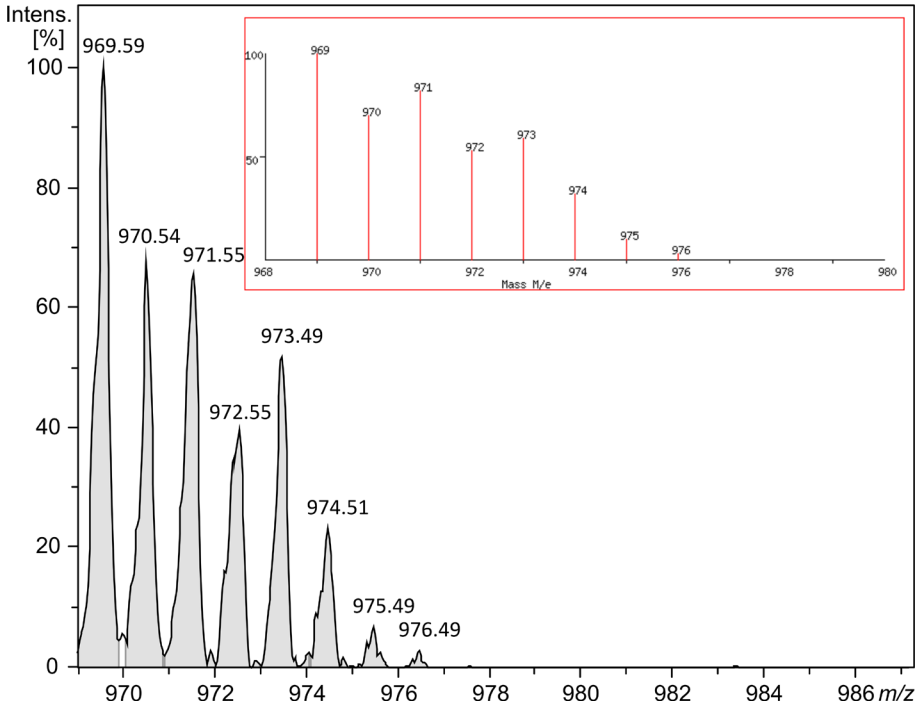

Fig. S5b The isotopic resolved part of the ESI/MS spectra of complex **5** measured in MeOH in the region involving the peak at 969.59 *m/z*, corresponding to $[Zn(Lap)(bphen)_2]^+$ (the red bordered inset represents the theoretical isotopic distribution pattern for this species).

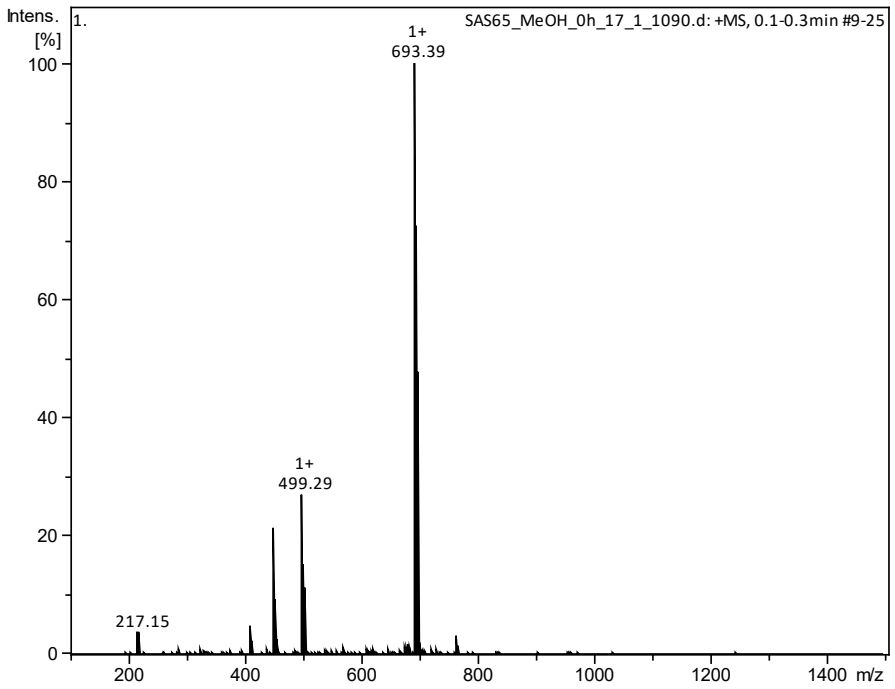

Fig. S6 ESI-MS spectrum of complex **6** measured in MeOH using the positive ionisation mode immediately after the sample dissolution. The main peaks represent the following pseudomolecular ions (theor. monoisotopic mass): 499.29 *m/z* $[Zn(Lap)(mphen)]^+$ (499.10); 693.39 *m/z* $[Zn(mphen)_2]^+$ (693.18).

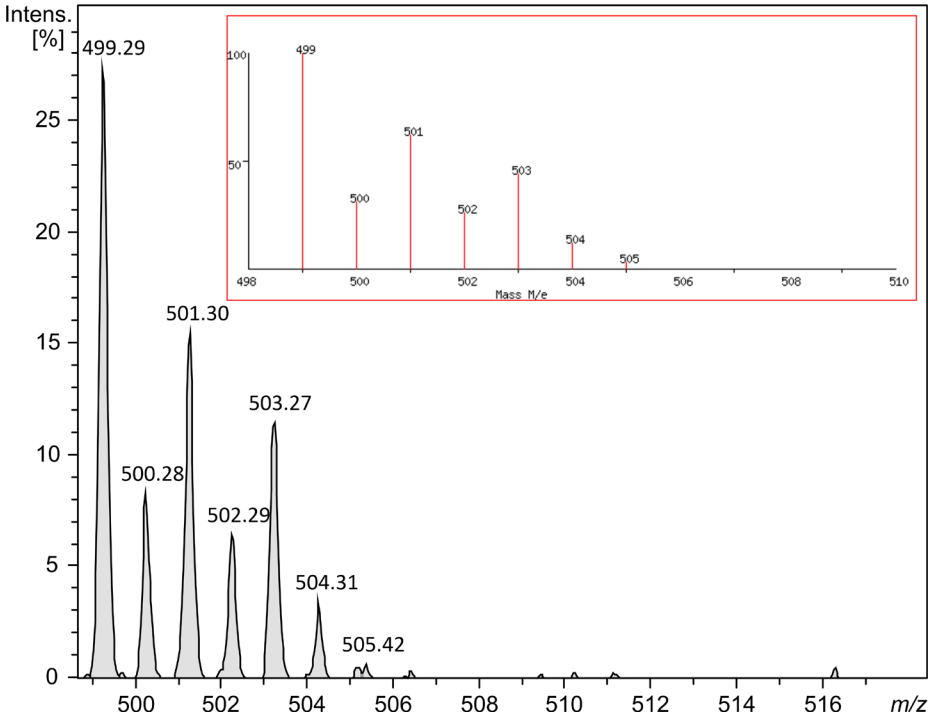

Fig. S6a The isotopic resolved part of the ESI/MS spectra of complex **6** measured in MeOH in the region involving the peak at 499.29 *m/z*, corresponding to $[Zn(Lap)(mphen)]^+$ (the red bordered inset represents the theoretical isotopic distribution pattern for this species).

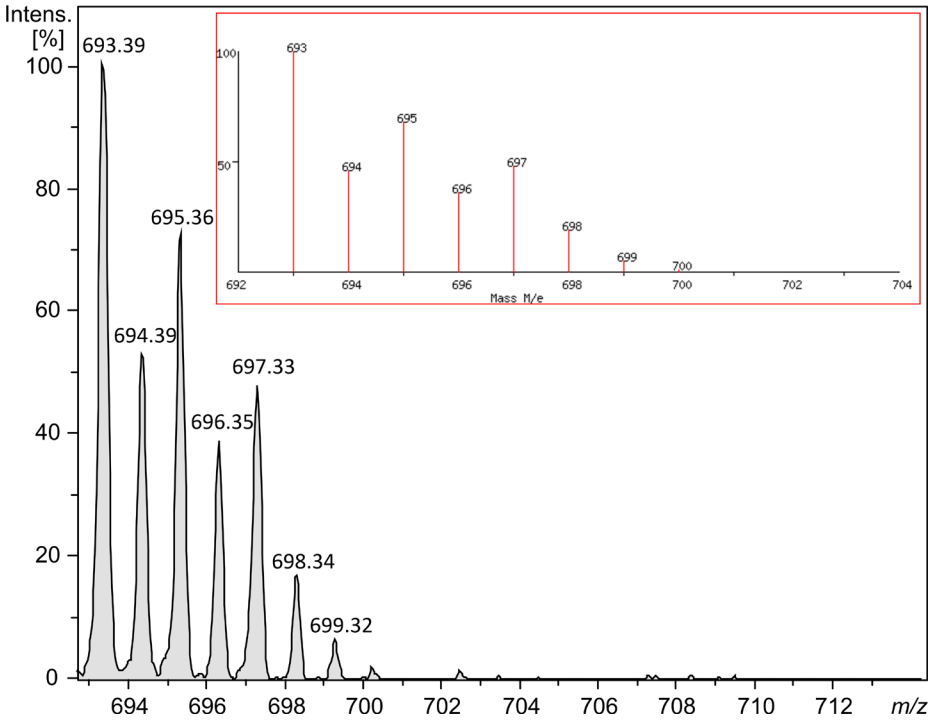

Fig. S6b The isotopic resolved part of the ESI/MS spectra of complex **6** measured in MeOH in the region involving the peak at 693.39 *m/z*, corresponding to $[Zn(Lap)(mphen)_2]^+$ (the red bordered inset represents the theoretical isotopic distribution pattern for this species).

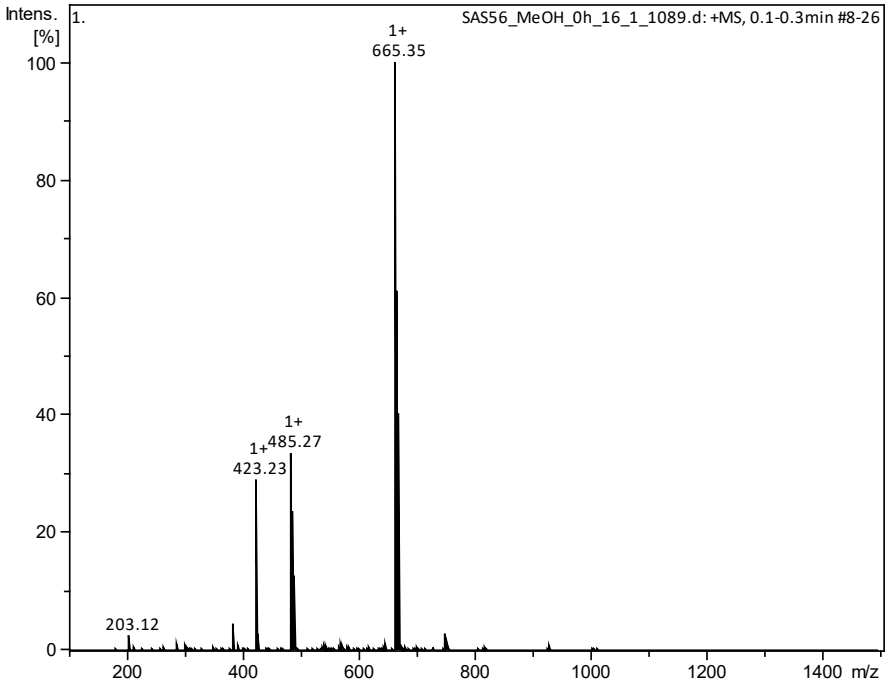

Fig. S7 ESI-MS spectrum of complex **7** measured in MeOH using the positive ionisation mode immediately after the sample dissolution. The main peaks represent the following pseudomolecular ions (theor. monoisotopic mass): 485.27 *m/z* $[Zn(Lap)(phen)]^+$ (485.08); 665.35 *m/z* $[Zn(Lap)(phen)_2]^+$ (665.15).

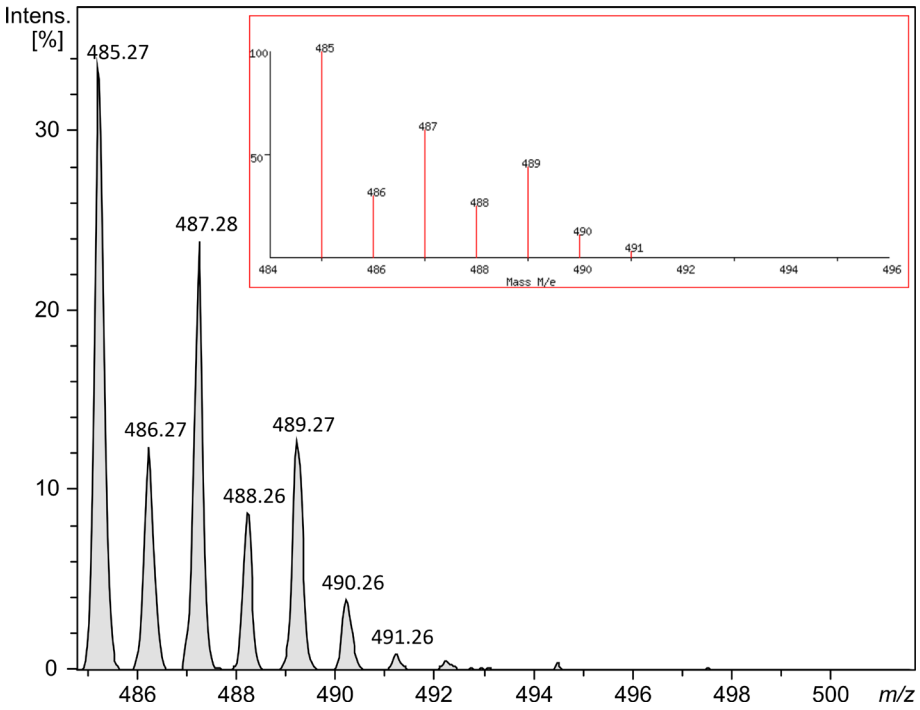

Fig. S7a The isotopic resolved part of the ESI/MS spectra of complex **7** measured in MeOH in the region involving the peak at 485.27 *m/z*, corresponding to $[Zn(Lap)(phen)]^+$ (the red bordered inset represents the theoretical isotopic distribution pattern for this species).

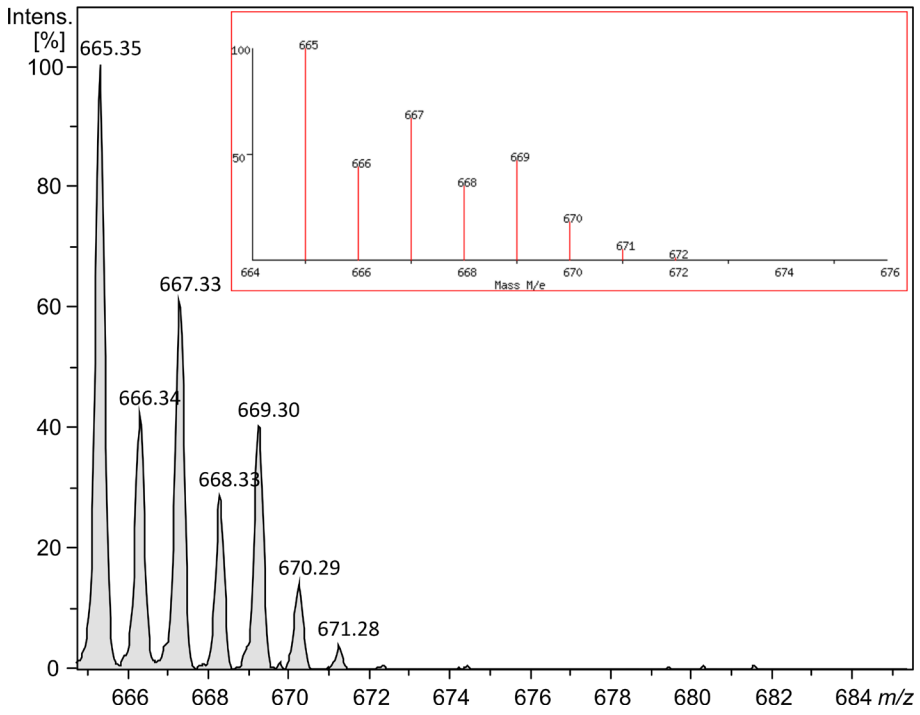

Fig. S7b The isotopic resolved part of the ESI/MS spectra of complex **7** measured in MeOH in the region involving the peak at 665.35 *m/z*, corresponding to $[Zn(Lap)(phen)_2]^+$ (the red bordered inset represents the theoretical isotopic distribution pattern for this species).

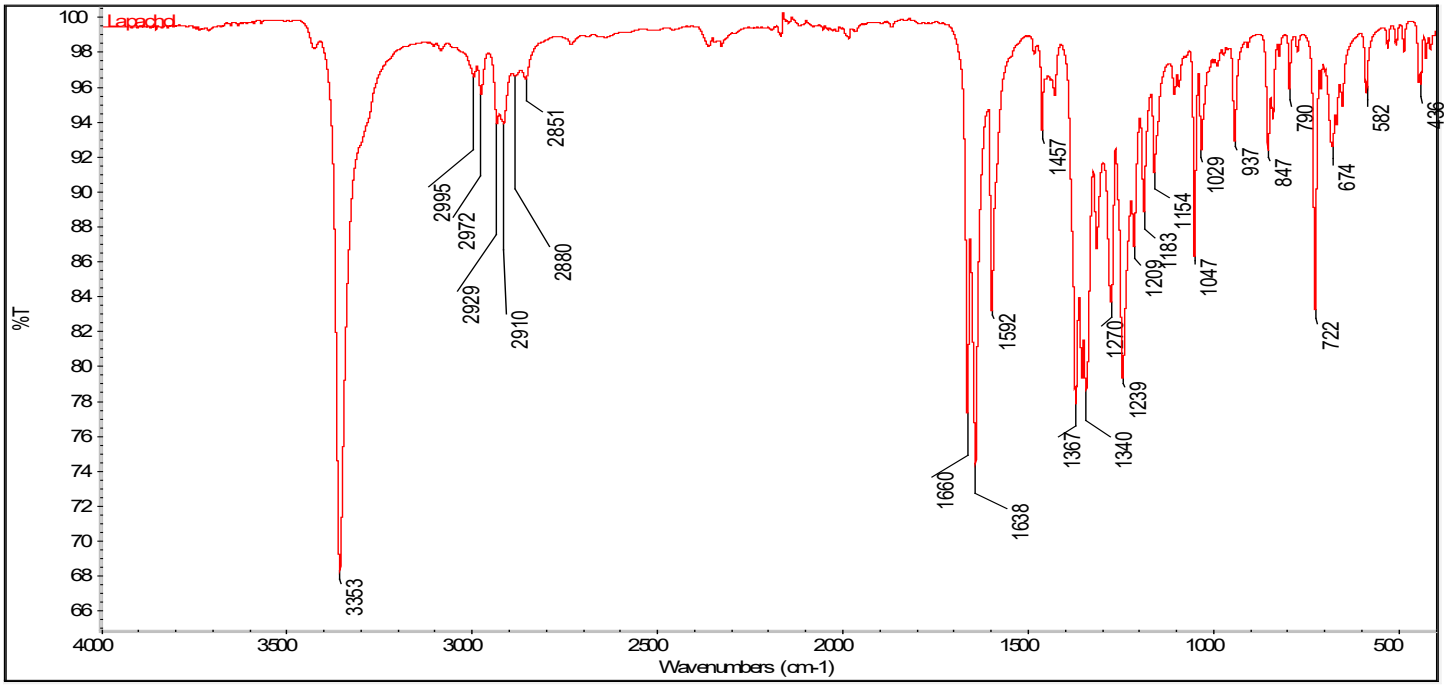

Fig. S8 IR spectrum of free Lapachol (HLap).

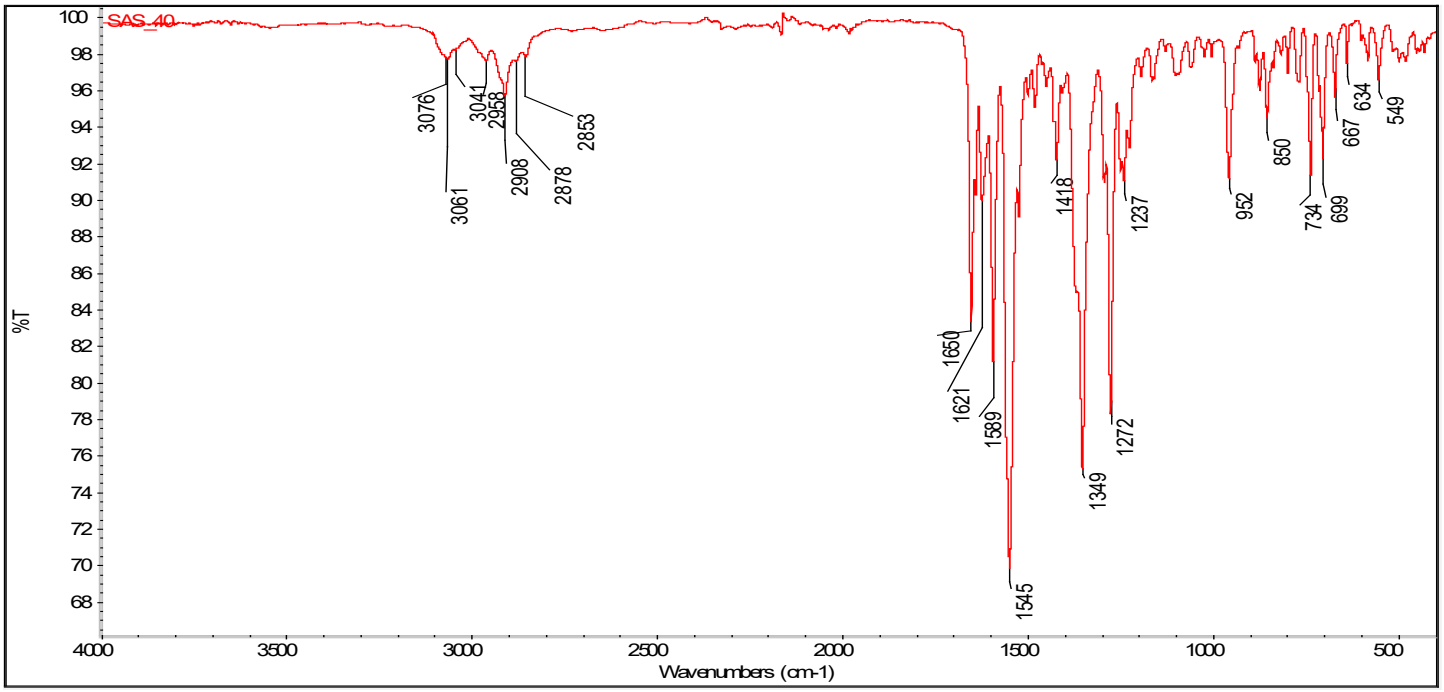

Fig. S9. IR spectrum of complex **1**.

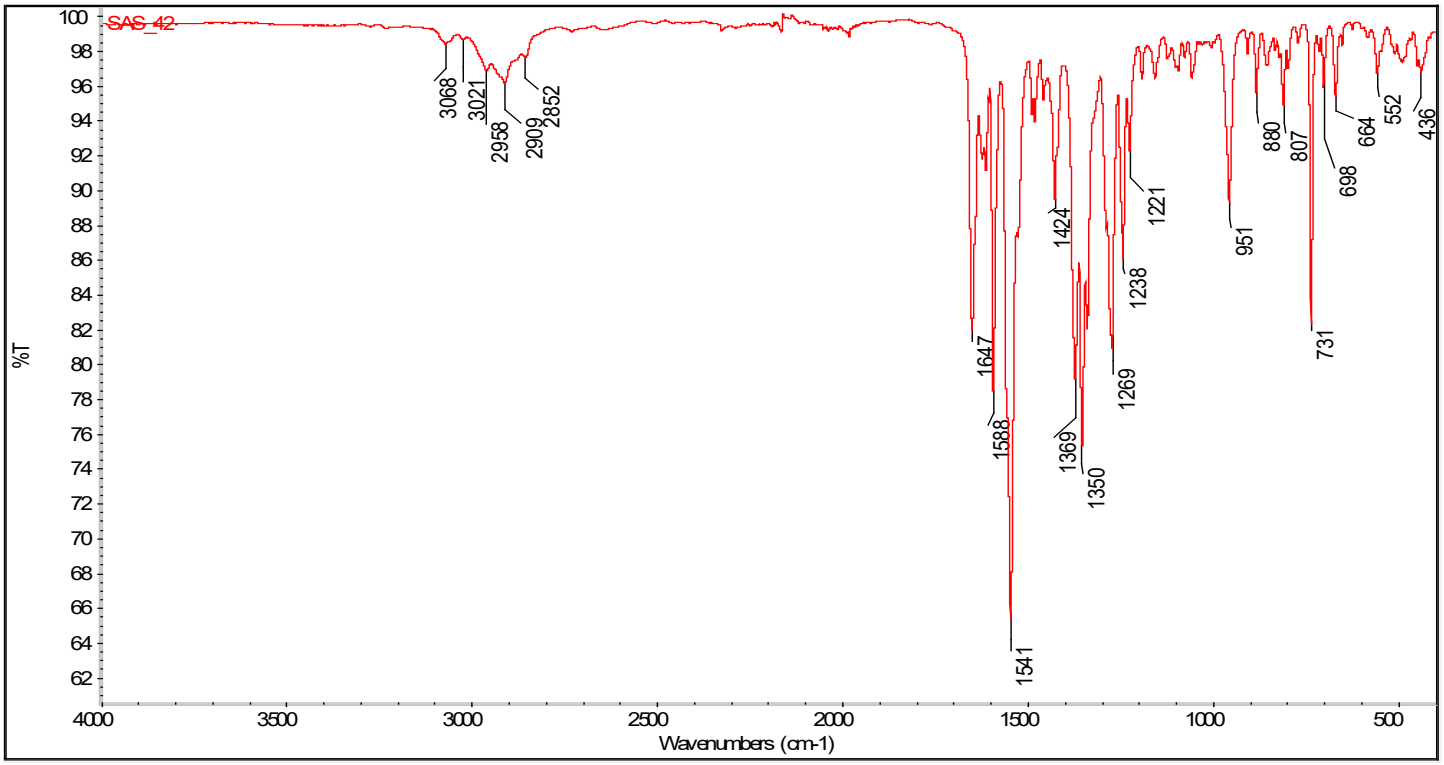

Fig. S10. IR spectrum of complex **2**.

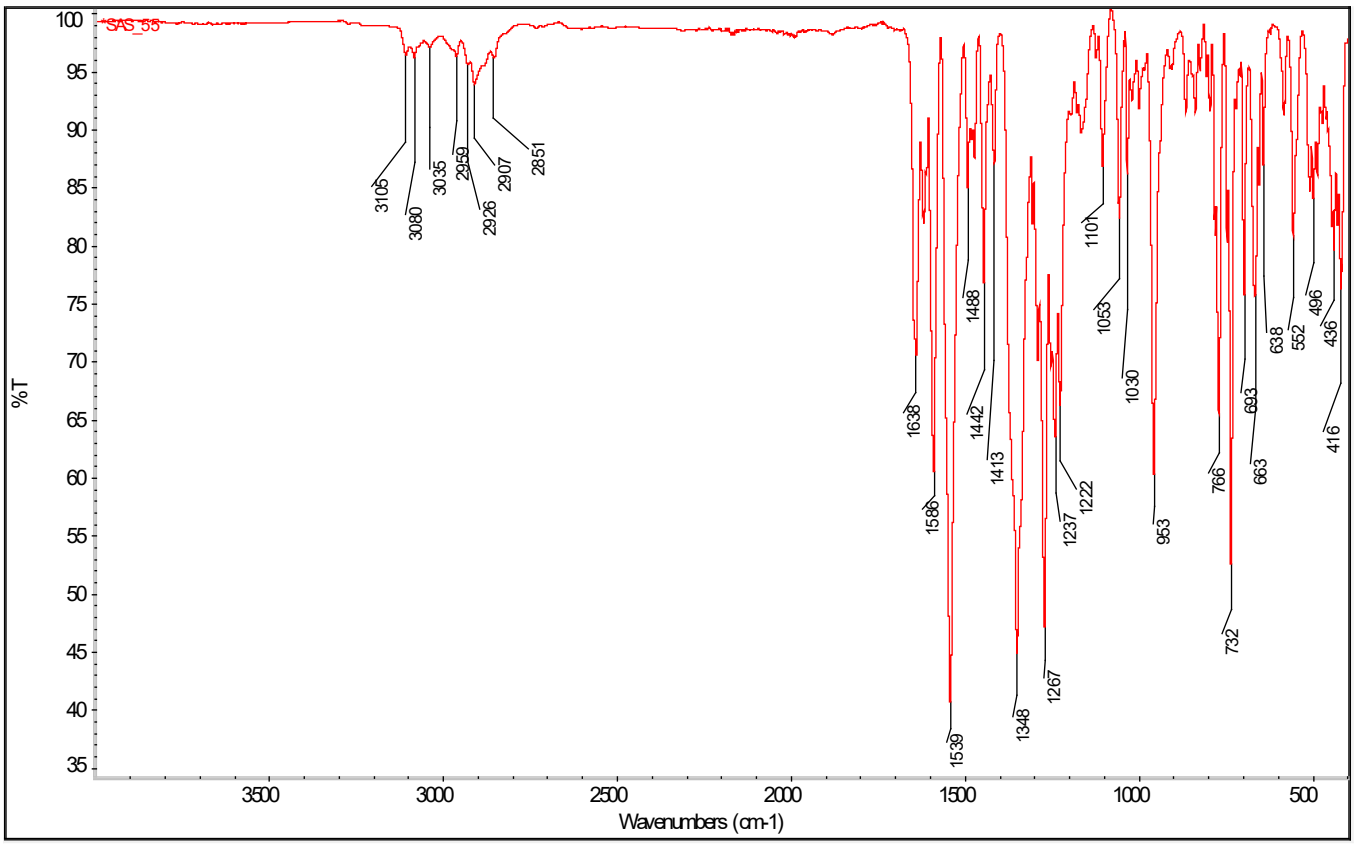

Fig. S11. IR spectrum of complex **3**.

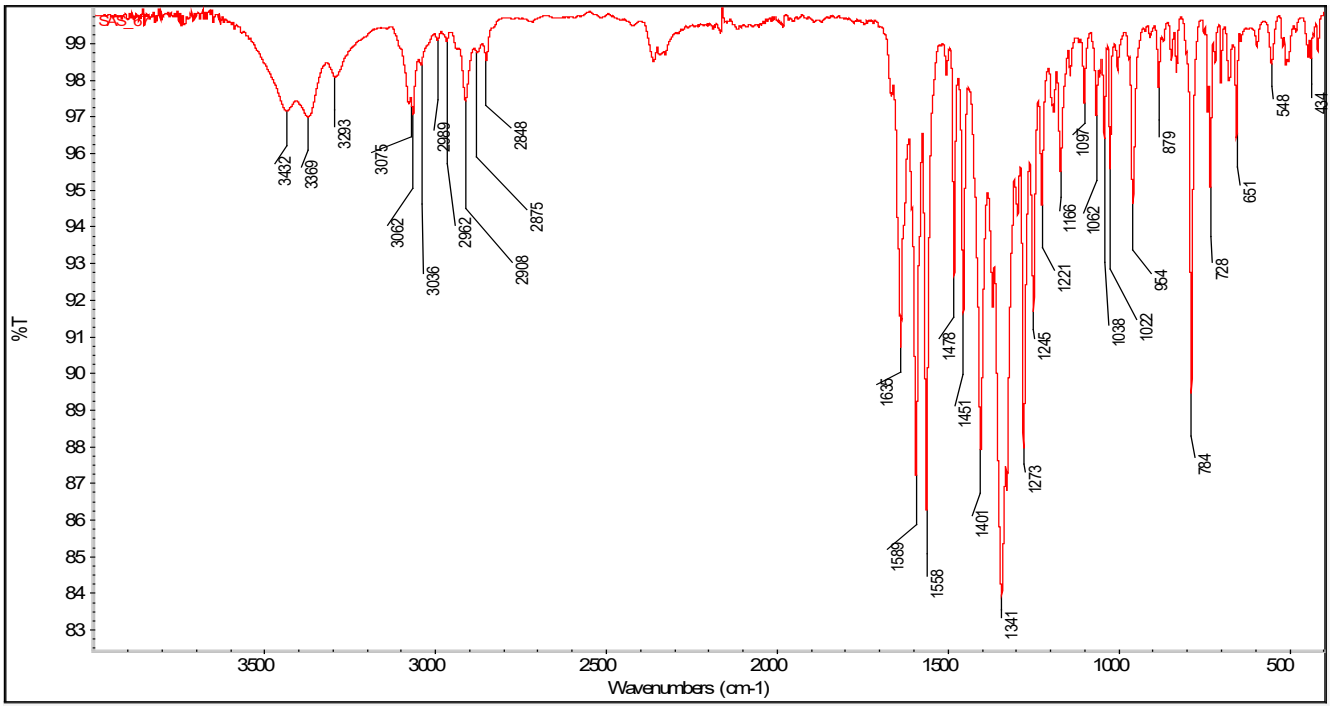

Fig. S12. IR spectrum of complex **4**.

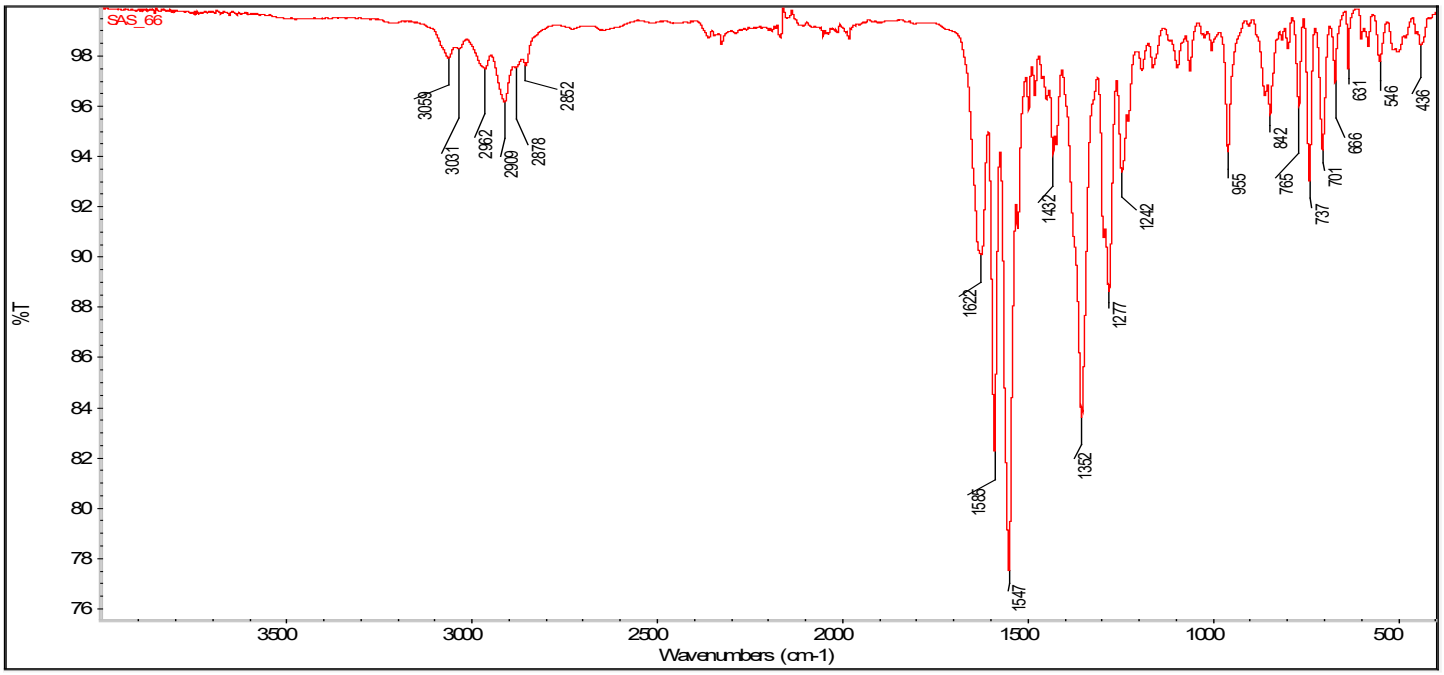

Fig. S13. IR spectrum of complex **5**.

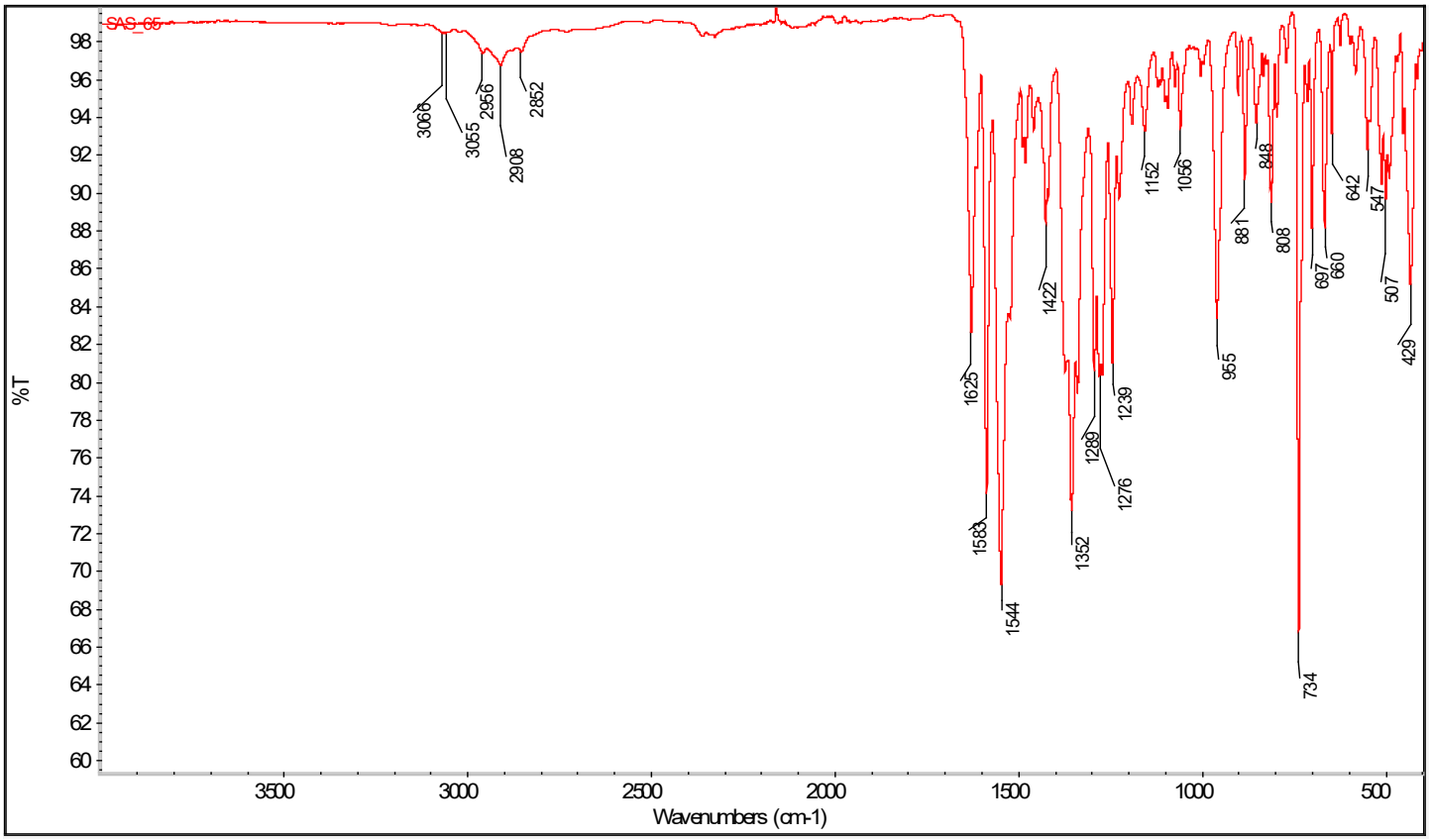

Fig. S14. IR spectrum of complex **6**.

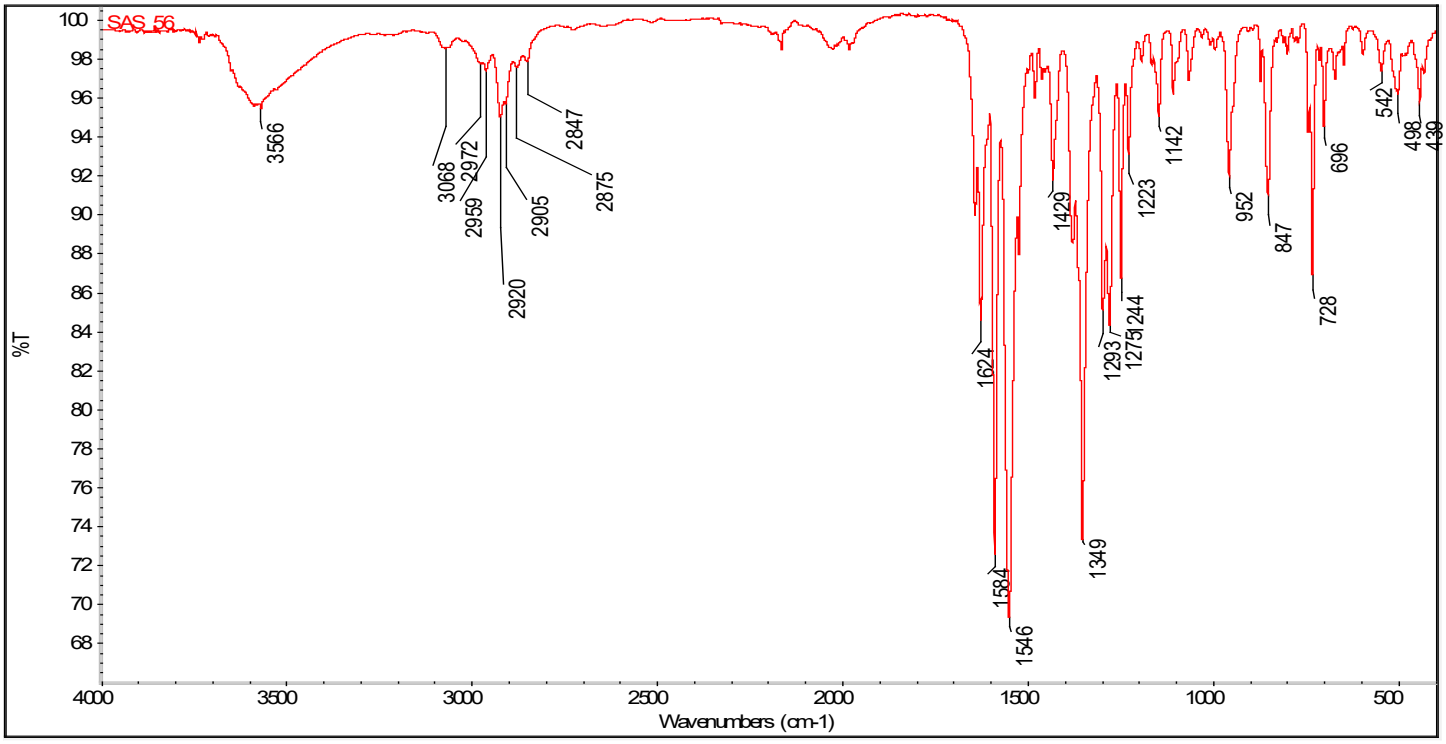

Fig. S15. IR spectrum of complex **7**.

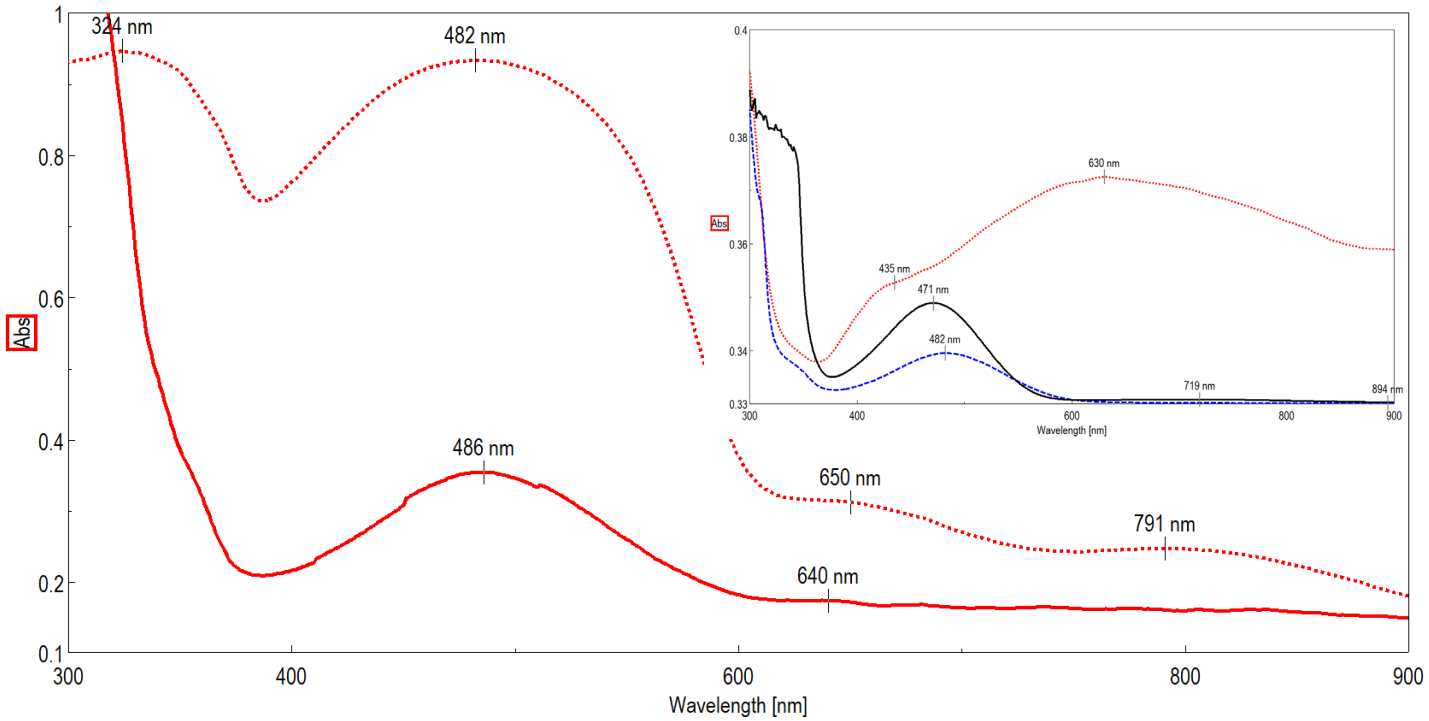

Fig. S16. Electronic spectra of complex **1** measured in the solid state (red solid line) and MeOH (red dashed line) together with spectra of complexes **2** (red dotted line), **3** (blue dashed line) and **4** (black full line) measured in MeOH (inset).

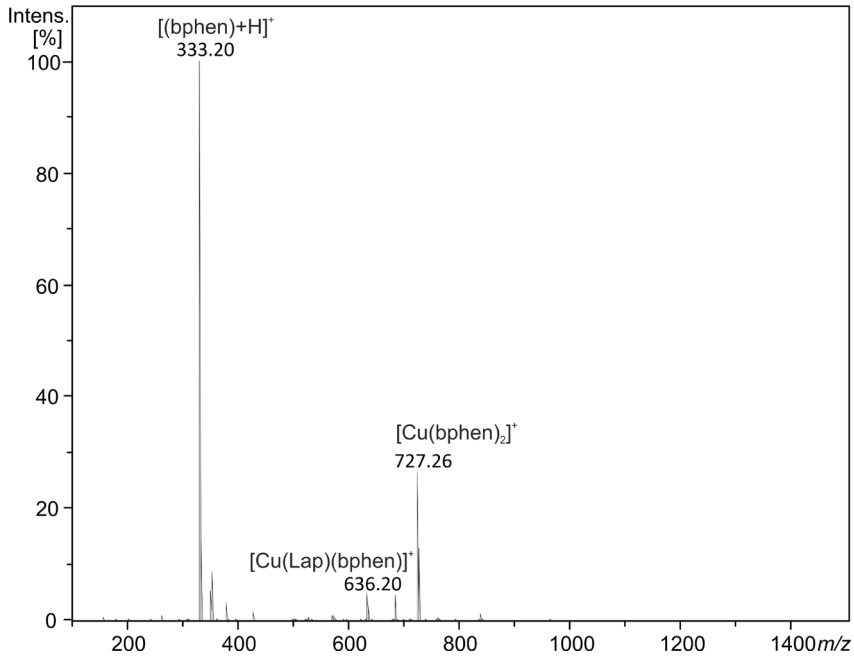

Fig. S17 ESI-MS spectrum of complex **1** measured in MeOH:H_2O (1:1) using the positive ionisation mode immediately after the sample preparation. The main peaks represent the following pseudomolecular ions: 333.20 *m/z* [(bphen)+H]$^+$; 636.20 *m/z* [Cu(Lap)(bphen)]$^+$; 727.26 *m/z* [Cu(bphen)$_2$]$^+$.

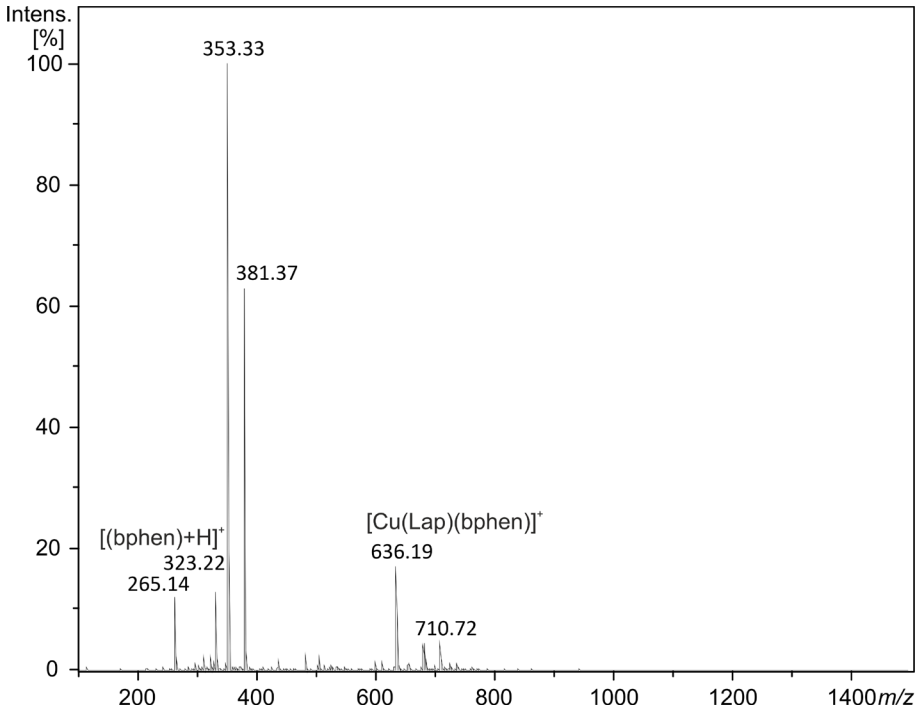

Fig. S18 ESI-MS spectrum of complex **1** measured in MeOH:H_2O (1:1) using the positive ionisation mode 24 h after the sample preparation. The main peaks represent the following pseudomolecular ions: 333.22 *m/z* $[(bphen)+H]^+$; 636.19 *m/z* $[Cu(Lap)(bphen)]^+$.

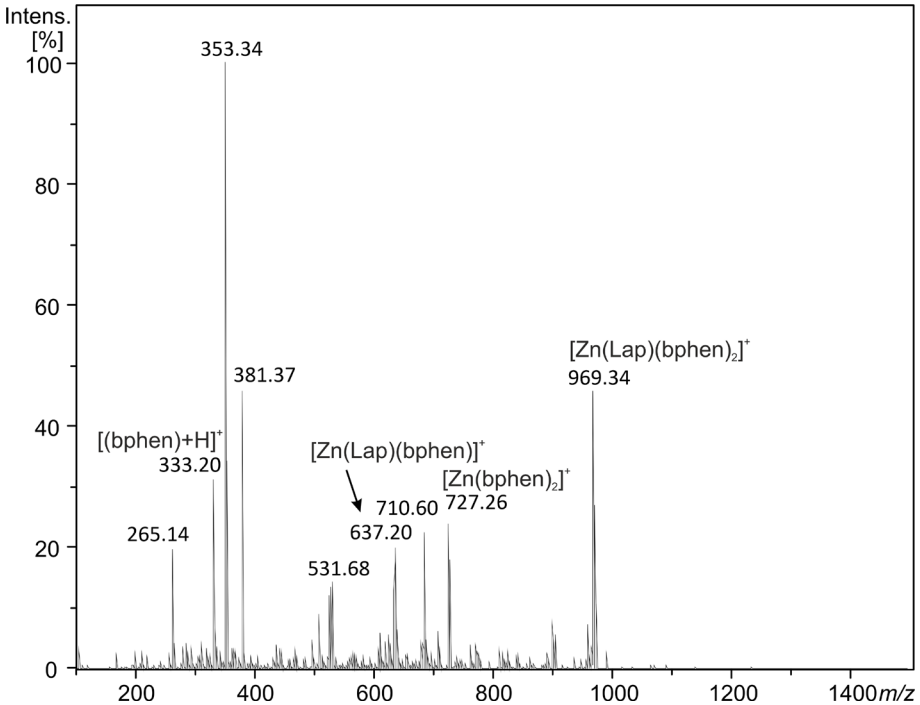

Fig. S19 ESI-MS spectrum of complex **5** measured in MeOH:H_2O (1:1) using the positive ionisation mode immediately after the sample preparation. The main peaks represent the following pseudomolecular ions (theor. monoisotopic mass): 333.20 *m/z* $[(bphen)+H]^+$; 637.20 *m/z* $[Zn(Lap)(bphen)]^+$; 727.26 *m/z* $[Zn(bphen)_2]^+$; 969.34 *m/z* $[Zn(Lap)(bphen)_2]^+$.

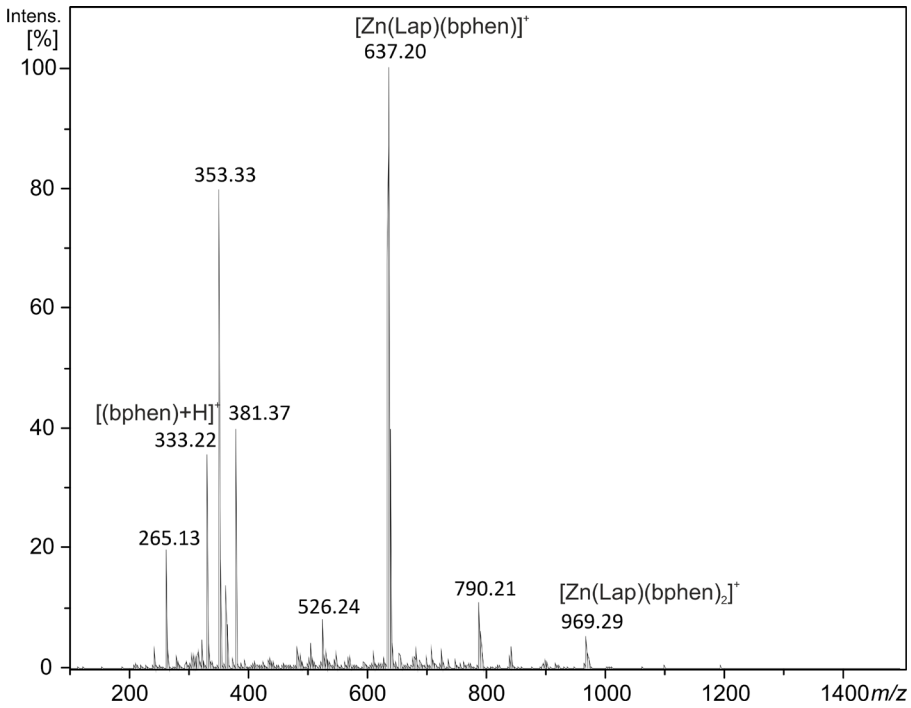

Fig. S20 ESI-MS spectrum of complex **5** measured in MeOH:H_2O (1:1) using the positive ionisation mode 24 h after the sample preparation. The main peaks represent the following pseudomolecular ions (theor. monoisotopic mass): 333.22 *m/z* $[(bphen)+H]^+$; 637.20 *m/z* $[Zn(Lap)(bphen)]^+$; 969.29 *m/z* $[Zn(Lap)(bphen)_2]^+$.

Table S1 Crystal data and structure refinements for **4**, **5,** and **6**

Complex	**4**	**5**	**6**
Empirical formula	C_{39} H_{26} Cu N_4 O_7	C_{54} H_{42} Zn N_2 O_6	C_{43} H_{36} Zn N_2 O_6
Formula weight	618.09	880.26	742.11
Temperature, K	293(2)	293(2)	293(2) K
Wavelength, Å	0.71073	0.71073	0.71073
Crystal system	Monoclinic	Triclinic	Monoclinic
Space group	$P2_1/c$	P-1	$P2_1/n$
Unit cell dimensions, Å and °	a = 8.269(8) b = 40.45(5) c = 9.081(10) α = 90.0 β = 112.25(3) γ = 90.0	a = 12.533(6) b = 13.657(6) c = 14.655(7) α = 104.069(15) β = 106.86(2) γ = 100.62(3)	a = 10.625(10) b = 14.831(16) c = 22.80(2) α = 90 β = 93.00(5) γ = 90
Volume, Å^3	2811(6)	2239.1(19)	3588(6)
Z	4	2	4
Density (calculated), g/cm^3	1.461	1.306	1.374
Absorption correction	Multi-scan	Multi-scan	Multi-scan
Absorption coefficient, mm^{-1}	0.832	0.602	0.737
F(000)	1276	916	1544
Crystal size, mm	0.10 x 0.10 x 0.04	0.20 x 0.16 x 0.16	0.14 x 0.12 x 0.12
θ range for data collection, °	2.01 to 26.42	1.89 to 23.54	2.07 to 23.83
Index ranges	$-9\le h\le 10$, $-45\le k\le 45$, $-9\le l\le 9$	$-14\le h\le 14$, $-15\le k\le 15$, $-16\le l\le 16$	$-12\le h\le 12$, $-16\le k\le 16$, $-25\le l\le 25$
Reflections collected	32674	40038	41743
Independent reflections	4316 [R(int) = 0.0989]	6642 [R(int) = 0.0947]	5508 [R(int) = 0.2341]
Completeness to θ	85.6 %	99.6 %	99.8 %
Refinement method	Full-matrix least-squares on F^2	Full-matrix least-squares on F^2	Full-matrix least-squares on F^2
Data / restraints / parameters	4316 / 0 / 393	6642 / 0 / 554	5508 / 0 / 455
Goodness-of-fit on F^2	1.272	1.027	1.021
Final R indices [$I>2\sigma(I)$]	$R1$ = 0.0582, $wR2$ = 0.1255	$R1$ = 0.0500, $wR2$ = 0.1056	$R1$ = 0.0755, $wR2$ = 0.1625
R indices (all data)	$R1$ = 0.0828, $wR2$ = 0.1341	$R1$ = 0.0882, $wR2$ = 0.1237	$R1$ = 0.1546, $wR2$ = 0.1970
Largest diff. peak and hole, e.Å^{-3}	1.419 and -1.369	0.615 and -0.666	1.028 and -1.160
CCDC number	2369949	2369950	2369951

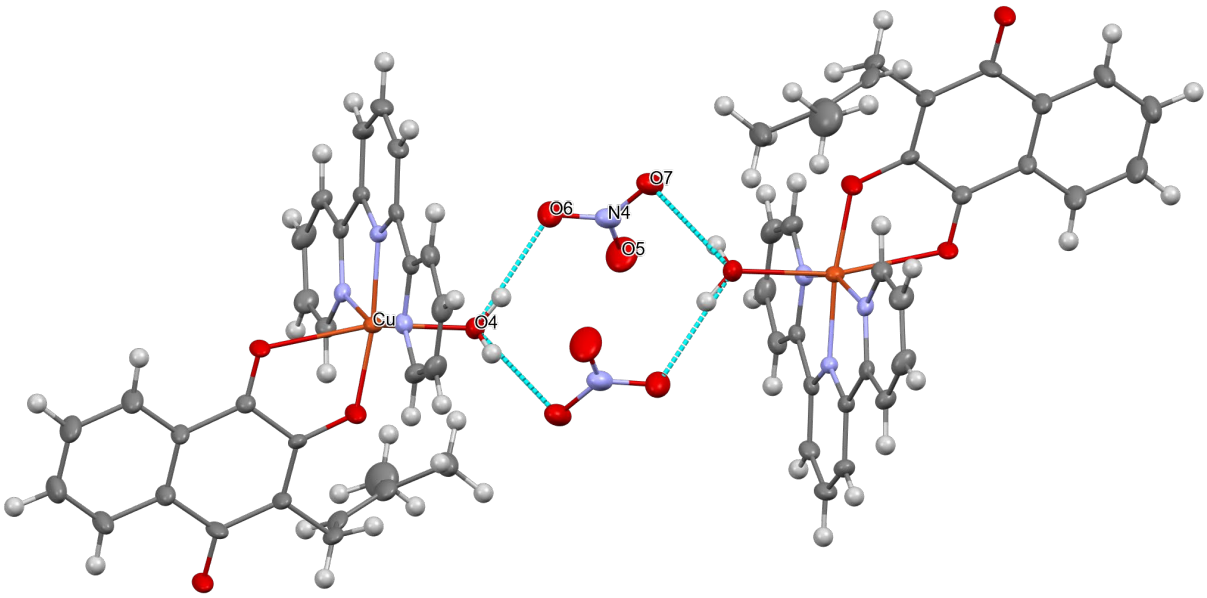

Fig. S21 The O–H···O hydrogen bonds (cyan dashed lines) connect centrosymmetrically two individual molecules of **4** through the nitrate anions.

Table S2 Parameters of selected hydrogen bonds [Å and °] in complex **4**.

D–H···A	d(D–H)	d(H···A)	d(D···A)	<(DHA)
O(4)–H(4W) ···N(4)	0.83(5)	2.69(5)	3.501(7)	164(5)
O(4)–H(4W)···O(6)	0.83(5)	1.97(5)	2.795(6)	170(5)
O(4)–H(4V)···O(7)#1	0.83(6)	2.07(6)	2.873(6)	162(5)
C(24)–H(24)···O(7)#2	0.93	2.55	3.416(7)	155.4
C(30)–H(30)···O(6)#3	0.93	2.20	3.120(6)	169.4
C(30)–H(30)···O(7)#3	0.93	2.65	3.195(7)	118.3

Symmetry transformations used to generate equivalent atoms: #1 -x+2,-y+1,-z+1; #2 -x+1,-y+1,-z; #3 -x+1,-y+1,-z+1.

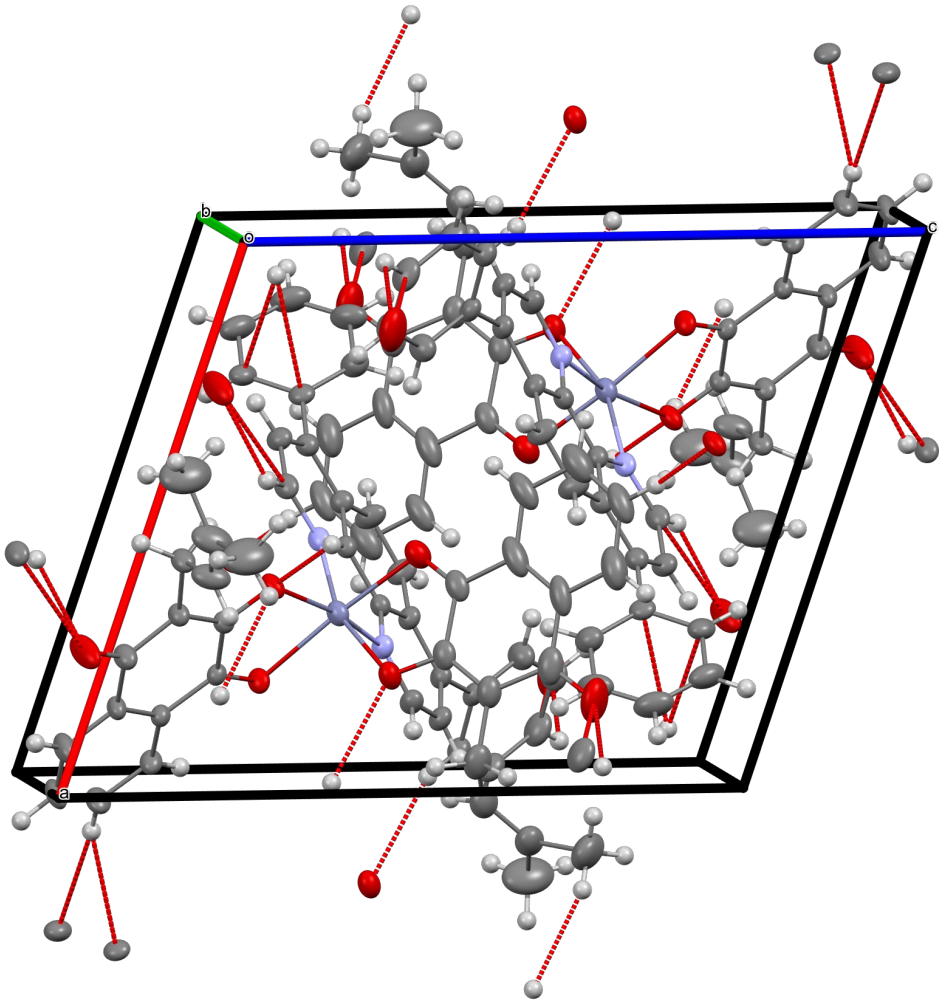

Fig. S22 Part of the crystal structure of **5**, showing the C–H···C and C–H···O non-covalent contacts (red dotted lines) connecting individual molecules of **5** into a 3D structure.

Table S3 Parameters of selected hydrogen bonds [Å and °] for complex **5**.

D-H···A	d(D-H)	d(H···A)	d(D···A)	<(DHA)
C(16)-H(16A)···O(6)#1	0.93	2.48	3.190(5)	133.7

Symmetry transformation used to generate equivalent atoms: #1 -x+1,-y,-z.

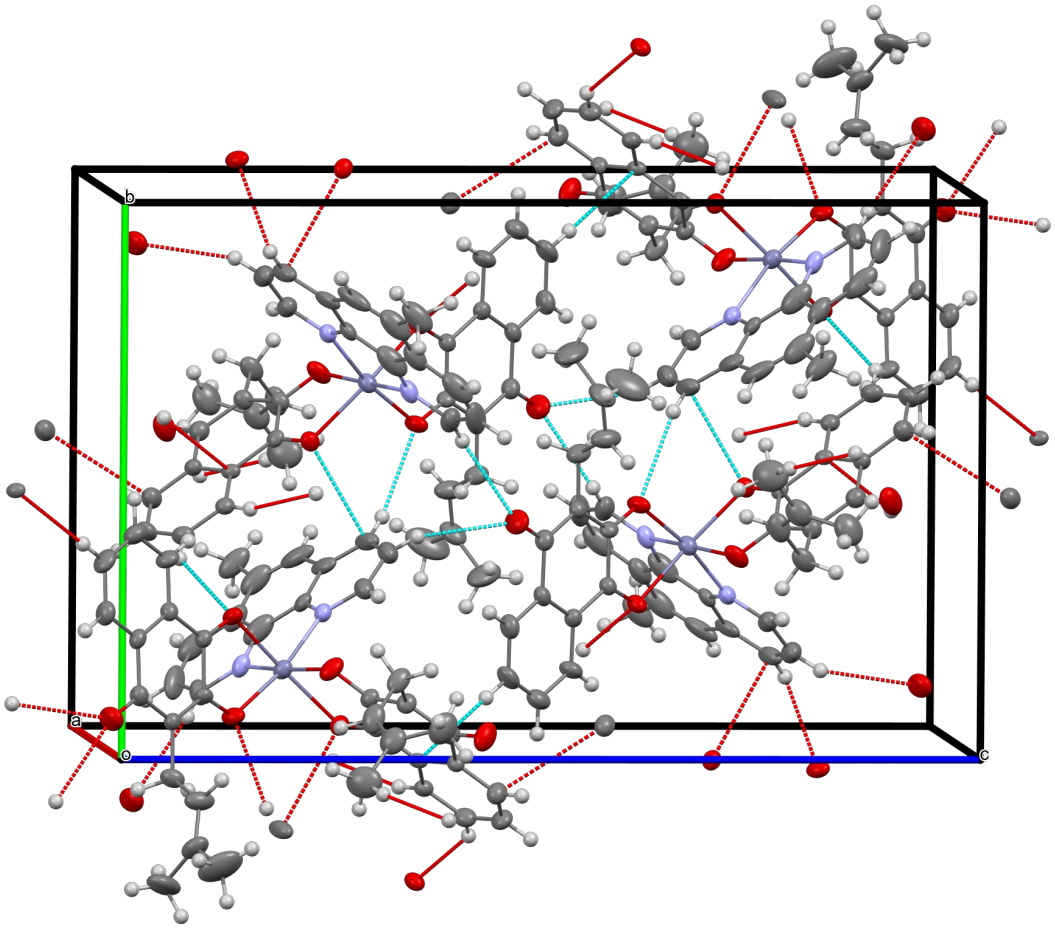

Fig. S23 Part of the crystal structure of **6**, showing the C–H···C, C–H···O (red dotted lines) and C···O (cyan dotted lines) non-covalent contacts, connecting individual molecules of **6** into a 3D structure.

Table S4 Parameters of selected hydrogen bonds [Å and °] for complex **6**.

D-H···A	d(D–H)	d(H···A)	d(D···A)	<(DHA)
C(26)–H(26A)...O(6)#1	0.93	2.66	3.473(11)	146.5

Symmetry transformation used to generate equivalent atoms: #1 -x+1,-y+1,-z+1.

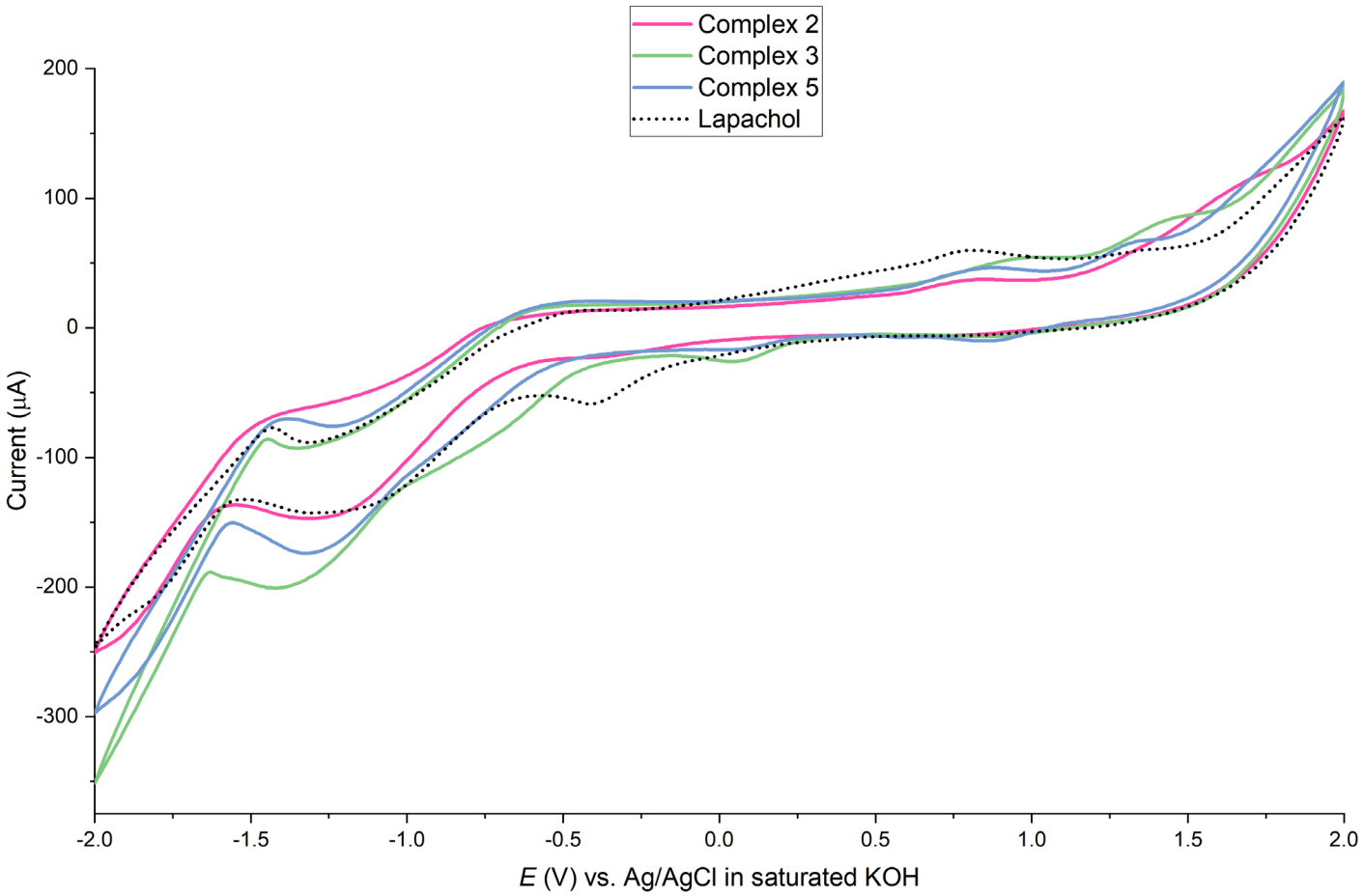

Fig. S24 The cyclic-voltammograms of complexes **2**, **3**, **5**, and ligand lapachol measured at 0.1 mM concentration in CH_2Cl_2 containing 0.1 M Bu_4NPF_6 as a supporting electrolyte using the Gamry Series G300 potentiostat (Gamry Instruments, Warminster, PA, USA) equipped with platinum foil working and counter electrode and Ag/AgCl in saturated KOH reference electrode.

Table S5 The potentials (V) of the maxima/shoulders of the anodic and cathodic waves (E_{pa} - anodic, E_{pc} - cathodic) vs. reference electrode Ag/AgCl in saturated KOH. The values were obtained by the analysis of the raw data using the Gamry Echem Analyst software (ver. 6.33).

Compound	Potentials of the wave maxima/shoulder (E_{pa} – anodic, E_{pc} – cathodic)						
	E_{pa1}	E_{pa2}	E_{pa3}	E_{pa4}	E_{pc1}	E_{pc2}	E_{pc3}
Lapachol	1.350	0.810	-0.400	-1.440	0.850	-0.420	-1.310
Complex **2**	1.340	0.880	-0.380	-1.390	0.850	0.020	-1.330
Complex **3**	1.450	1.030	-0.548	-1.450	0.850	0.040	-1.420
Complex **5**	0.840	-0.690	-1.430	-	0.630	-0.390	-1.310